Contents lists available at ScienceDirect

Transactions of Nonferrous Metals Society of China

36(2026) 571−585

www.tnmsc.cn

Improving mechanical properties of Cu/CNTs composites by incorporating nanotwins

Wei-lin YU [a,#], Si-wei LUO [a,#], Juan ZHU [a,#], Min SONG [b], Tian-yu SUN [a], Jian-hong YI [c], Liang LIU [c], Yang-zhen LIU [a], Zhi-guo ZHANG [a,*], Yong YANG [d], Zhen-tao YU [a], Wei LI [a], Bai-song GUO [a,**]

[a] Institute of Advanced Wear & Corrosion Resistant and Functional Materials, Jinan University, Guangzhou 510632, China;

[b] State Key Laboratory of Powder Metallurgy, Central South University, Changsha 410083, China;

[c] Faculty of Materials Science and Engineering, Kunming University of Science and Technology, Kunming 650093, China;

[d] Department of Mechanical Engineering, College of Engineering, City University of Hong Kong, Hong Kong 99907, China

Abstract: To exploit the combined strengthening effects of nanotwins and carbon nanotubes (CNTs) in Cu matrix composites, the nanotwins with a width ranging from 3 to 30 nm were incorporated into the CNTs-reinforced Cu matrix composites using cryogenic rolling and optimizing the initial particle size of the raw Cu powders. The formation of nanotwins in the Cu matrix composite reinforced by only 0.2 wt.% CNTs is accompanied by the increased dislocation density and refined Cu grain size, resulting in much better strength−ductility synergy than the referenced composite without significant nanotwins formation. The analysis of strengthening and toughening mechanisms demonstrates that the strength increment mainly derives from grain refinement strengthening, dislocation strengthening, and nanotwin strengthening. The strength increment from the contribution of the nanotwins accounts for 19.9% of the overall strength increment for the composite. Meanwhile, the retention of good tensile ductility can be reasonably explained by the increased dislocation accommodation ability due to the formed nanotwins and the decreased induced dislocation proliferation.

Keywords: Cu matrix composite; carbon nanotube; nanotwin; strength; ductility

1 Introduction

Due to their remarkable mechanical properties and excellent thermoelectric properties, carbon nanotubes (CNTs) reinforced Cu matrix composites have been regarded as a new generation of Cu matrix composites for vast industrial areas [1−4]. Achieving good dispersion of CNTs and a high bonding interface with Cu matrix are the two premises for fully exploiting the potential strengthening effects of CNTs for Cu matrix composites [5,6]. To date, many fruitful methods have been developed to improve the CNTs dispersion in the Cu matrix and to strengthen the Cu−CNTs interfacial bonding. However, the overall strength of CNTs/Cu composites is still far from the expectation, because the improvement of higher strength of Cu matrix has been ignored by most researchers. Grain refinement strengthening [7], solid solution strengthening [8], and precipitation strengthening [9] have been demonstrated to be effective approaches to improve the strength of Cu matrix materials, while the improved strength is generally accompanied by reduced ductility [10].

[#]Wei-lin YU, Si-wei LUO and Juan ZHU contributed equally to this work

Corresponding author: [*]Zhi-guo ZHANG, Tel: +86-13538885336, E-mail: zhigzhang@jnu.edu.cn;

[**]Bai-song GUO, Tel: +86-15700796463; E-mail: guobaisong@jnu.edu.cn

https://doi.org/10.1016/S1003-6326(25)66982-2

Received 27 May 2024; accepted 3 March 2025

To alleviate the contradiction between the strength and ductility of metal materials, a series of microstructure regulation methods have been proposed in the past two decades, such as incorporating the nanotwins by various approaches [11,12]. The findings show that twinning can synergistically increase the strength and toughness of Cu matrix materials, breaking the inverse relationship between the strength and toughness. For example, ZHAO et al [13] synthesized heterogeneous nanostructured Cu with a high density of nanotwins, showing a much higher strength and fracture toughness. However, almost all previous studies only focused on the effects of nanotwins on the mechanical properties of pure Cu, Cu alloy, and other metal materials, whereas the combined effects of nanotwins and ex-situ reinforcement for Cu matrix composites have not been explored yet.

To introduce nanotwins into metal materials including Cu, a series of means including direct-current electrodeposition, annealing, and plastic deformation have been developed by various researchers [14,15]. CHENG et al [16] proposed a direct-current electrodeposition technique and demonstrated that the width and density of nanotwins can be effectively controlled in pure Cu by precisely adjusting the processing parameters. However, the low fabrication efficiency of direct-current electrodeposition and micro-scaled sample size limit the application of such a method. Annealing is also a feasible approach to introduce the nanotwins into metal materials, due to the existing shear strain at grain boundaries and disclination-like lattice rotation induced by the grain growth during annealing [17]. MA et al [18] pointed out that annealing-induced nanotwins require high deformation energy, dense defects, and ultrafine grains, but these factors and the coarsening of nanotwins limit their strengthening effect. Unlike annealing and electrodeposition, plastic deformation can induce nanotwin formation on a large scale, especially in metals with low stacking fault energy. However, although it is common in bulk copper alloys and other metals, it is rarely used to promote the formation of nanotwins in Cu matrix composites. Recently, it has been found that the addition of CNTs into the FCC metal matrix can substantially lower its stacking fault energy and result in the formation of stacking faults [19]. So, it can be deduced that the CNTs reinforced Cu matrix composite might be easier to form nanotwins by plastic deformation than pure Cu. Nevertheless, the attempts to incorporate nanotwins into CNTs reinforced Cu matrix composites have not been reported so far.

In this study, the CNTs reinforced Cu matrix composites were fabricated by powder metallurgy route and subsequent hot rolling, which is effective in removing the residual pores after sintering [20]. Subsequently, cryogenic rolling was further applied to inducing the formation of Cu nanotwins in CNTs reinforced Cu matrix composites, because it has been demonstrated that the dislocation activity in the metal material was restricted in the cryogenic rolling process, thus facilitating the formation of nano-twins [21−23]. The microstructure and mechanical properties of the hot-rolled and subsequently cryogenically-rolled composites were investigated, and the involved strengthening and toughening mechanisms were also deeply discussed. The findings of this study can guide the microstructure regulation of the CNTs reinforced Cu matrix composites for higher mechanical properties.

2 Experimental

2.1 Purification and surface functionalization of CNTs

The CNTs with high purity (>98%) as used in our previous study [24] were employed for present CNTs reinforced Cu matrix composites. To remove the commonly residual catalyst particles, the raw CNTs were immersed in a mixed acid reagent (67 wt.% HNO_3 and 98 wt.% H_2SO_4 with a volume ratio of 1∶3) for 0.5 h at 50 °C, the magnetic stirring was applied to enhancing the purification effect, the acid-treated CNTs were then collected by vacuum filtration and washed with deionized water to neutral pH. The collected CNTs were further oxidized in another mixed acid reagent (67 wt.% HNO_3 and 98 wt.% H_2SO_4 with volume ratio of 3∶1) for 5 h at 50 °C under magnetic stirring to functionalize the CNTs with oxygen-containing functional groups. The oxygen-containing functional groups were attached to the surface of CNTs to promote the CNTs dispersion in Cu powders during the subsequent composite powder preparation process.

2.2 Fabrication of bulk CNTs reinforced Cu matrix composite

The coarse (~50 μm) and fine (~5 μm) Cu

powders in spherical shapes were sieved from the Cu powders prepared by Ar gas atomization [25]. Then, 90 g of Cu powders consisting of 50 wt.% coarse Cu powders and 50 wt.% fine Cu powders (C_1F_1) were mixed with the 0.2 wt.% acid-treated CNTs (0.16 g) by alcohol-assisted ball milling. The same parameters as in our previous study [2] were used for the ball milling mixing process and subsequent sintering and hot rolling. The hot-rolled composites were named as HR-C_1F_1. For comparison, the composite using 100 wt.% fine Cu powders (C_0F_1) as the matrix powders was fabricated using identical processes and named HR-C_0F_1. To induce the formation of nanotwins in the two types of composites, part of the hot-rolled specimens were rolled after immersing in liquid nitrogen for 10 min. The rolling direction was parallel to the hot rolling direction, and the height reduction after six passes rolling was about 30%. Finally, the specimens obtained by cryogenic rolling were annealed at 200 °C for 1 h followed by cooling in the furnace. The two types of cryogenically-rolled specimens were correspondingly named HCR-C_1F_1 and HCR-C_0F_1, respectively. The details about the nomenclature of the specimens are listed in Table 1.

Table 1 Nomenclature of specimens

Specimen	Raw powders composition	Plastic deformation process
HR-C_0F_1	100 wt.% fine Cu powders	Hot rolling
HR-C_1F_1	50 wt.% coarse Cu powders + 50 wt.% fine Cu powders	Hot rolling
HCR-C_0F_1	100 wt.% fine Cu powders	Hot rolling + cryogenic rolling
HCR-C_1F_1	50 wt.% coarse Cu powders + 50 wt.% fine Cu powders	Hot rolling + cryogenic rolling

2.3 Characterization of microstructure and mechanical properties

The morphologies of the composite powders were examined using a scanning electron microscope (SEM, Hitachi SU8000) operated at 3 kV. The phase information of bulk composites was characterized by X-ray diffraction (XRD, Rigaku UItima IV) using a Cu K_α radiation source (λ=1.54178 Å). The XRD scanning voltage was 40 kV, the tube current was 40 mA, and the scanning rate and 2θ range were 5 (°)/min and 10°−100°, respectively.

The structural information of the Cu matrix was analyzed by an electron backscatter diffraction (EBSD) system attached to a JEOL-JSM-IT800 SEM. The EBSD samples were prepared by mechanical polishing with diamond suspensions followed by fine polishing using a Fischione 1061 ion mill. The continually adjusted processing voltage and time were 8 V, 30 min; 4 V, 30 min; 2 V, 2 min; 2 V, 2 min. The average copper grain size, local strain distribution, and Schmid factor were analyzed based on the obtained EBSD data using Aztec software.

The microstructures including the CNTs−Cu interface and nanotwins in the fabricated composites were characterized by a transmission electron microscope (TALOS F200X, Thermo Fisher Scientific) operated at 200 kV, and the equipped EDS system was used to analyze the elemental distribution in the selected area. The TEM samples with the thin area that the electron beam can penetrate were prepared by mechanical milling followed by ion thinning at 5 kV using a Gatan Model 695 precision ion polishing system.

To evaluate the tensile properties of the composites, tensile specimens with a cross-section of 5 mm × 3 mm and a length of 10 mm were cut from the rolled sheets using wire-cutting, and the length direction of the tensile specimens was parallel to the rolling direction. The tensile tests were carried out at room temperature using an Instron 3369 tester with a strain rate of 2.1×10^{-3} s^{-1}. To confirm the repeatability of tensile properties, at least three tensile tests were carried out for each type of composite. After the tensile tests, tensile fractured surfaces of composites were observed by scanning electron microscopy (SEM, FEI Nova Nano 230) operated at 5 kV.

3 Results and discussion

3.1 Microstructures of powders and bulk composites

Figure 1 shows the SEM images of the two types of composite powders. As seen in Figs. 1(a) and (b), the raw spherical Cu powders are completely transformed into Cu flakes, due to the mechanical impaction of stainless-steel balls during the applied ball milling processes. Moreover, the cold welding coarsens the Cu flakes, increasing the average particle sizes of fine and coarse Cu flakes to ~30 μm

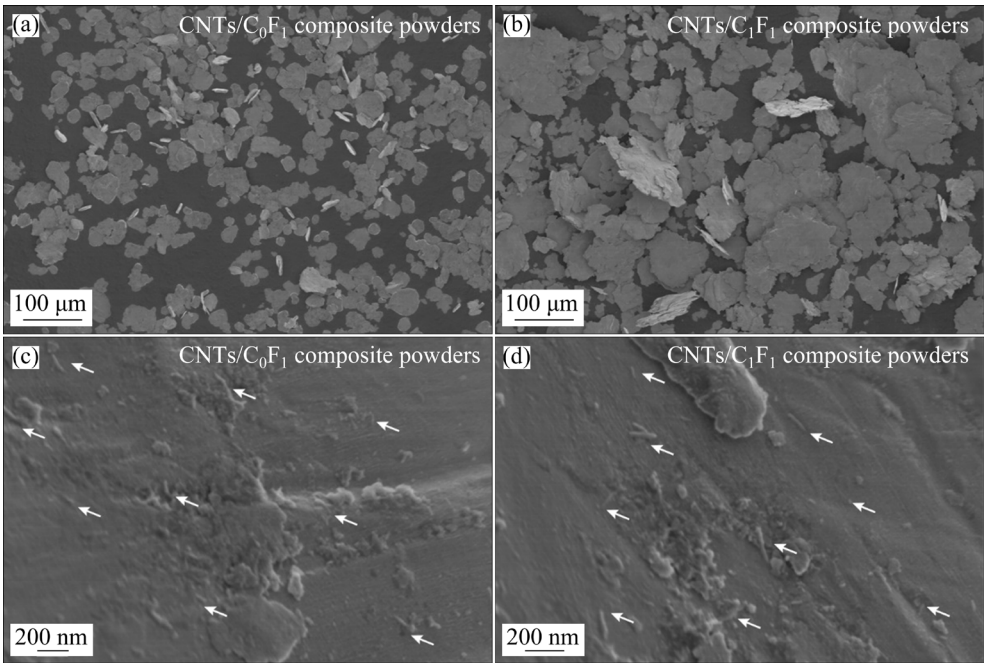

Fig. 1 SEM images with low and high magnifications of two composite powders: (a, c) CNTs/C_0F_1; (b, d) CNTs/C_1F_1 (The representative CNTs are marked by white arrows)

and ~120 μm, respectively. With further magnification (Figs. 1(c) and (d)), it can be detected that the CNTs are singly embedded in the Cu flakes and part of some CNTs are exposed outside the Cu flakes. Such observations confirm that the applied composite powder fabrication processes are effective in realizing the uniform dispersion and intragranular location of CNTs in the Cu matrix.

Figure 2 shows the XRD patterns of the as hot-rolled (HR-C_0F_1 and HR-C_1F_1) and further cryogenically-rolled (HCR-C_0F_1 and HCR-C_1F_1) composites. In the XRD patterns of the four bulk composites, several diffraction peaks at 43.31°, 50.45°, 74.12°, and 89.94° can be observed, which can be labeled as (111), (200), (220), and (311) crystalline planes of Cu, respectively, according to the PDF cards (PDF#85- 1326). The diffraction peaks of CNTs are not detected here due to their high dispersion and relatively low content. In addition, as shown in the inset, the addition of 50 wt.% coarse Cu powders (HR-C_1F_1) shifts the peak belonging to Cu(111) crystalline plane to the location with larger 2θ, while further cryogenic rolling significantly lowers the 2θ of Cu(111) crystalline plane for the two composites. Such peak shift characteristics denote that the incorporation of coarse Cu powders can reduce the dislocation density of the fabricated composites, and the cryogenic rolling results in substantial dislocation propagation and storage [26].

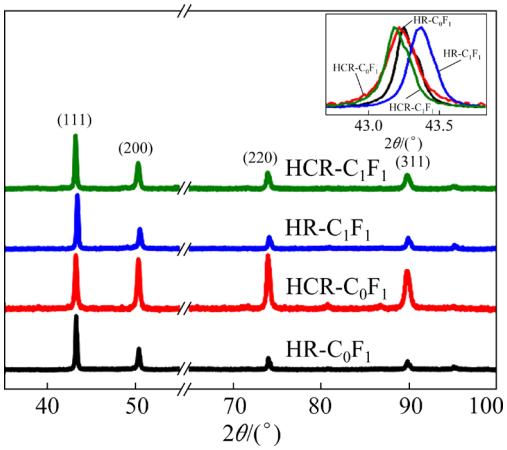

Fig. 2 XRD patterns of four types of fabricated composites (The insert is the amplified peak belonging to Cu(111) crystalline plane)

Figure 3 shows the EBSD inverse pole figures (IPFs) and statistical grain size results of the four types of composites. As shown in Figs. 3(a) and (b), both Cu matries of HR-C_0F_1 and HR-C_1F_1 composites consist of equiaxed grains with large-angle grain boundaries, denoting that the applied sintering and hot rolling processes induce the complete recrystallization. However, as for the HCR-C_0F_1 (Fig. 3(c)) and HCR-C_1F_1 (Fig. 3(d)), the color gradient can be observed in the interior of the retained equiaxed grains, implying that the low-angle grain boundary is formed by the grain rotation during the cryogenic rolling. Specifically, the

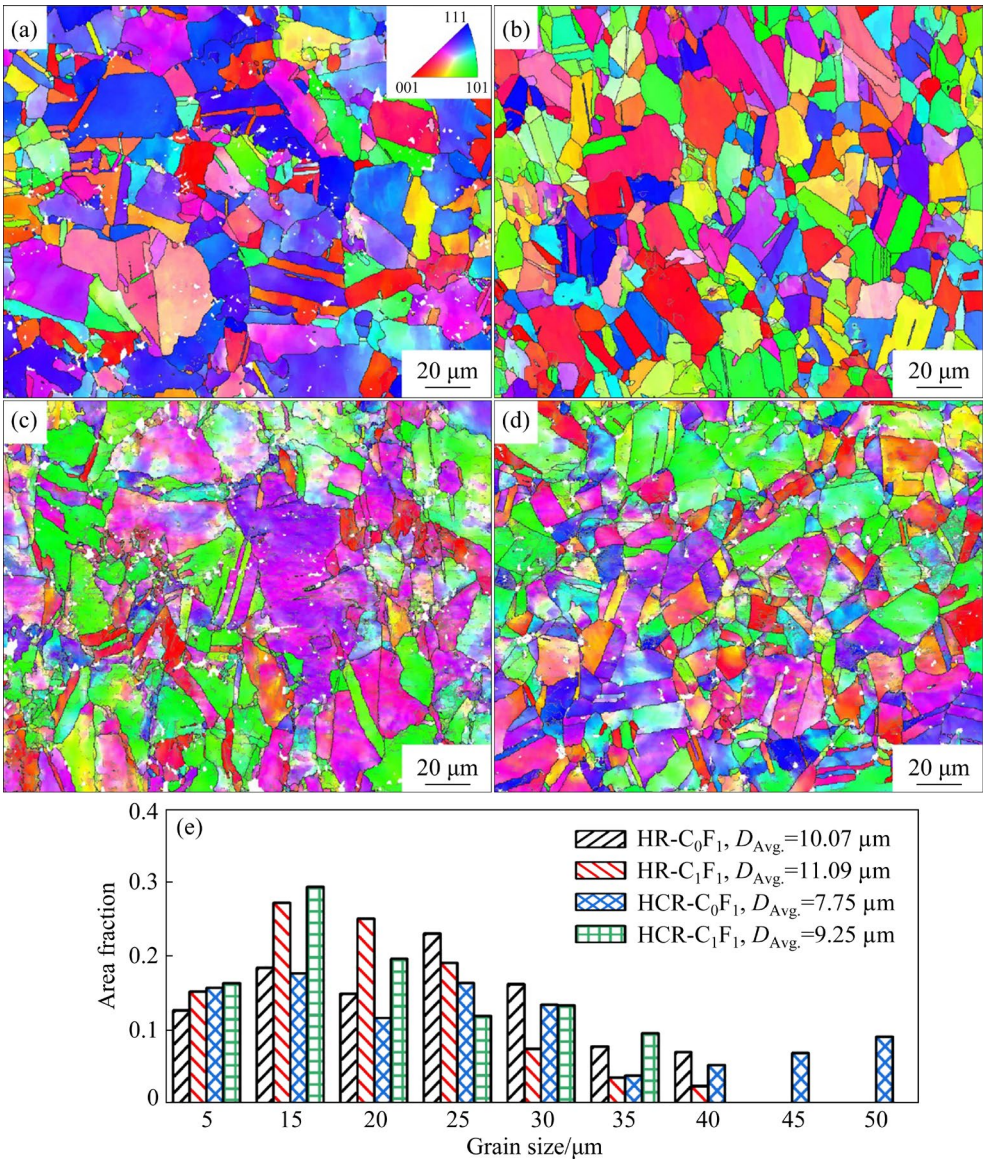

Fig. 3 EBSD IPFs and statistical grain size results of four types of composites: (a) HR-C_0F_1; (b) HR-C_1F_1; (c) HCR-C_0F_1; (d) HCR-C_1F_1; (e) Statistical grain size results

proportion of low-angle grain boundary in HCR-C_1F_1 is higher than that in HCR-C_0F_1, because the coarse grains are easier for local deformation and rotation. Moreover, as shown by the statistical grain size results, the average grain size of HR-C_1F_1 (11.09 μm) is slightly higher than that of HR-C_0F_1 (10.07 μm) (Fig. 3(e)). The minimized grain size difference further demonstrates that the two composites indeed experienced complete grain recrystallization and growth. In addition, the applied cryogenic rolling can refine the Cu grains to be 7.75 μm for HCR-C_0F_1 and 9.25 μm for HCR-C_1F_1. The grain refinement after cryogenic deformation has been commonly observed in Cu [27] and other metallic materials [28,29], because the deformation under low temperatures can substantially induce the dislocation multiplication and interaction as well as the formation of dislocation walls, which can be developed into grain boundaries, thus refining the grain.

The Schmid factor can be used to assess the probability of slip initiation (difficulty of deformation) of crystalline material in a given slip system for a single-crystal material. The average Schmid factor ($\overline{m}$) characterizes the difficulty of slip in plastic deformation of polycrystalline materials. The higher the value of $\overline{m}$, the easier the slip and the better the material's plasticity. Accordingly, as shown in Figs. 4(a−d) and (e, f), the Schmid factor of the HR-C_1F_1 is slightly higher than that of the

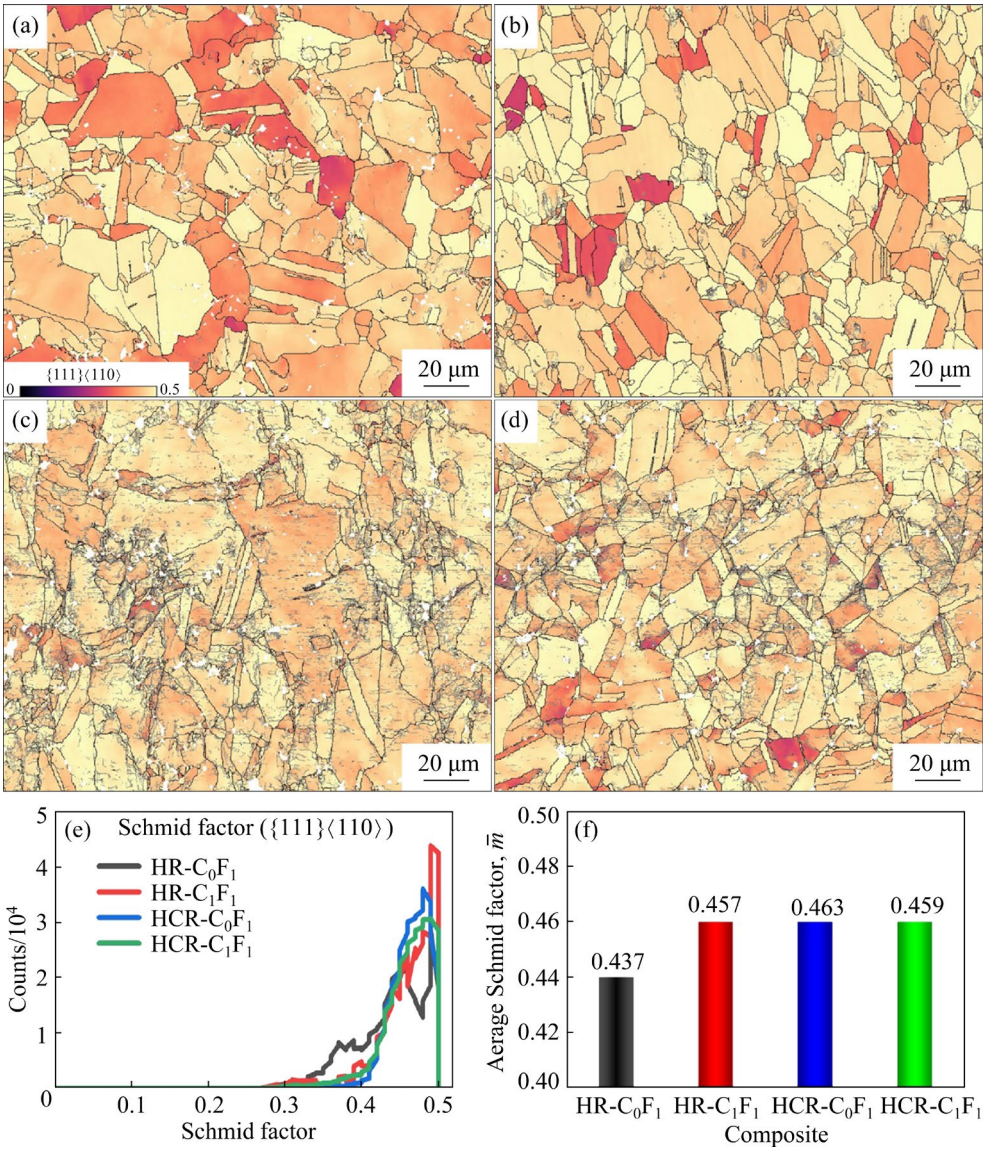

Fig. 4 Schmid factor analysis results of four types of composites: (a−d) Schmid factor maps of HR-C_0F_1, HR-C_1F_1, HCR-C_0F_1 and HCR-C_1F_1, respectively; (e, f) Statistical results of Schmidt factors

HR-C_0F_1, which suggests that the addition of coarse copper powder facilitates the slip of specific slip systems, thus benefiting the achievement of better plastic deformation ability. After cryogenic rolling, the difference in $\bar{m}$ between the HCR-C_0F_1 and HCR-C_1F_1 composites is negligible, which means that the influence of the slip system on the plastic deformation characteristics can be ignored for the two composites.

Meanwhile, the geometrically necessary dislocation (GND) maps of the four types of composites were analyzed and shown in Fig. 5. As presented in Figs. 5(a) and (b), the GND density of HR-C_1F_1 is lower than that of HR-C_0F_1. The coarse grain can accommodate more dislocation multiplication during plastic deformation and thus lower the GND density [30]. Furthermore, the GND density substantially increased in HCR-C_0F_1 and HCR-C_1F_1 after cryogenic rolling (Figs. 5(c) and (d)). The highly increased GND density can be attributed to two main reasons. On the one hand, the applied cryogenic rolling can induce GND multiplication more significantly in the Cu matrix than hot rolling, especially in the region around the Cu−CNTs interface, because the Cu matrix has much lower deformation ability at low temperatures. On the other hand, the low temperature can effectively suppress the dislocation recovery, thus leading to obvious dislocation accumulation. The corresponding statistical results are illustrated in Figs. 5(e) and (f),

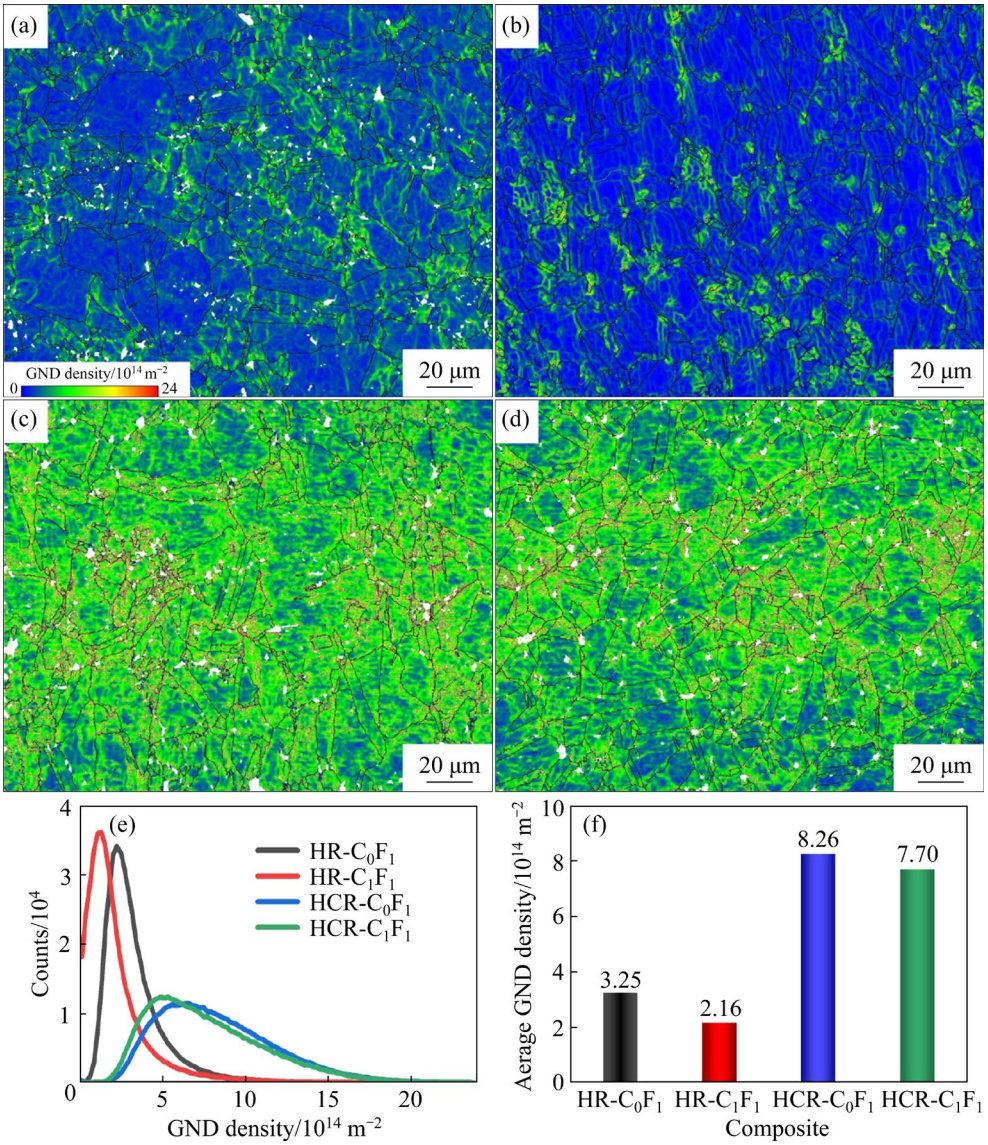

Fig. 5 GND analysis results of four types of composites based on EBSD characterization: (a−d) GND maps of HR-C_0F_1, HR-C_1F_1, HCR-C_0F_1, and HCR-C_1F_1, respectively; (e, f) Statistic results of GND density

showing that the average GND densities in HR-C_0F_1, HR-C_1F_1, HCR-C_0F_1, and HCR-C_1F_1 composites are 3.25×10^{14}, 2.16×10^{14}, 8.26×10^{14}, and 7.70×10^{14} m^{-2}, respectively. This GND density variation implies that cryogenic rolling can induce larger dislocation accumulation strengthening compared to hot rolling.

Figures 6(a−c) present the microstructures of the HR-C_0F_1 composite revealed by TEM. It can be seen that the CNTs have a good dispersion and distribute along the rolling direction in the HR-C_0F_1 composite (Fig. 6(a)), forming a tortuous and tight interface with the Cu matrix (Fig. 6(b)). Moreover, the Cu matrix has relatively high dislocation accumulation (Fig. 6(c)). Similarly, the CNTs in the HR-C_1F_1 also have uniform dispersion (Fig. 6(d)) and flexuous interface (Fig. 6(e)) with the Cu matrix. However, the density of accumulated dislocations in HR-C_1F_1 (Figs. 6(d) and (e)) is much lower than that in HR-C_0F_1. In addition, some deformed twins with twisted twin boundaries (Figs. 6(e) and (f)) can be detected in the HR-C_1F_1. The micro-area strain distributions of the interfacial region shown in Figs. 6(b) and (e) are further analyzed by the geometrical phase analysis (GPA) algorithm [31], and the analyzed strain fields (ε_{xx}, ε_{xy}, ε_{yx}, and ε_{yy}) are illustrated in Figs. 6(g) and (h). It can be seen that both the interface regions of HR-C_0F_1 and HR-C_1F_1 have a uniform strain distribution, which can be attributed to the dislocation and strain recovery during the hot rolling. The low local strain facilitates

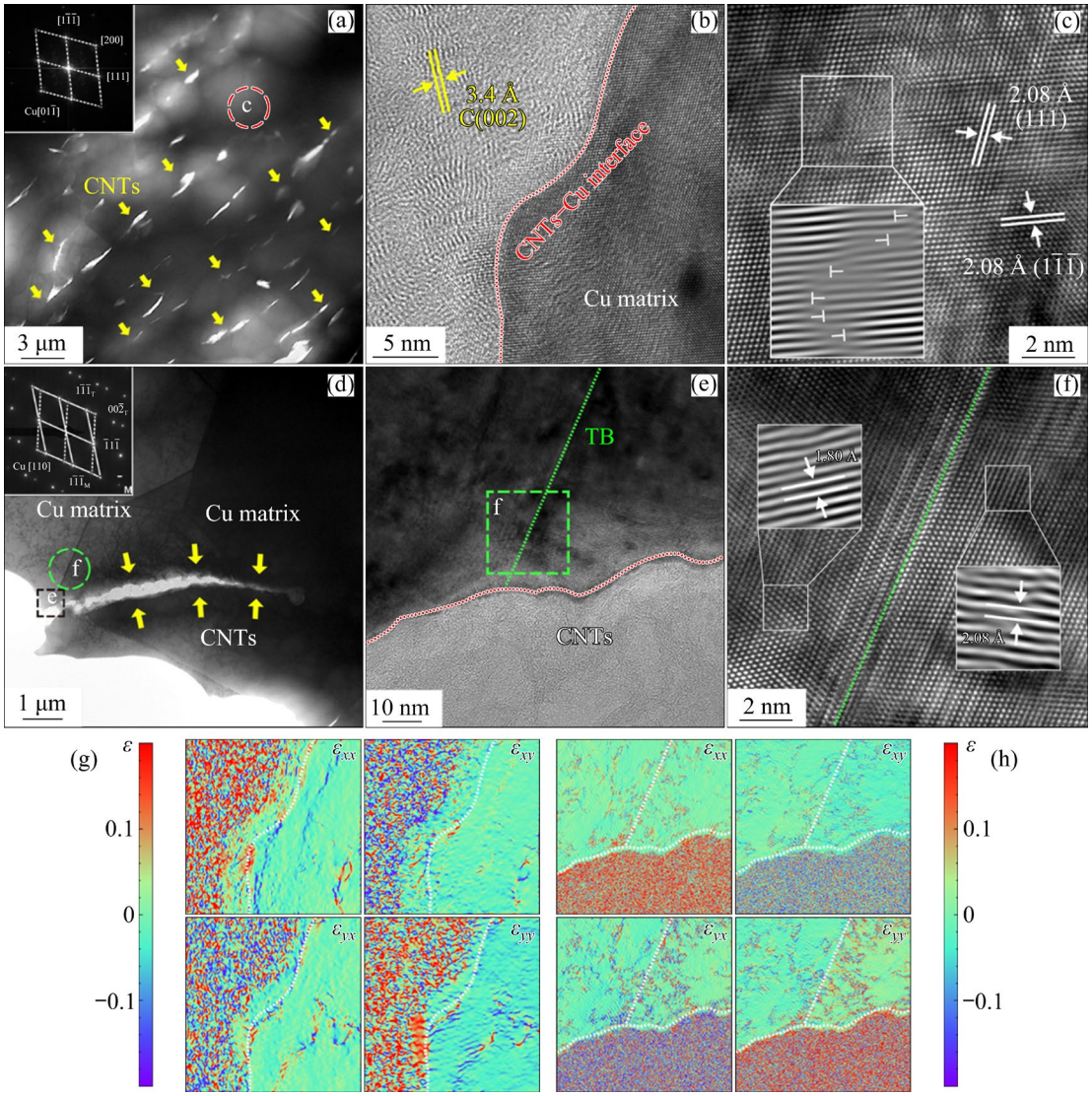

Fig. 6 Microstructures of HR-C_0F_1 and HR-C_1F_1 revealed by TEM (a−f) and corresponding local strain analysis results of Cu−CNTs interface (g, h): (a) Bright field TEM (BFTEM) image of HR-C_0F_1; (b) High-resolution TEM (HRTEM) image of Cu−CNTs interface in HR-C_0F_1; (c) HRTEM image of Cu matrix in HR-C_0F_1; (d) BFTEM image of HR-C_1F_1; (e) HRTEM image of Cu−CNTs interface in HR-C_1F_1; (f) HRTEM image of twin boundary in HR-C_1F_1; (g, h) Local strain distributions of Cu−CNTs interfaces of HR-C_0F_1 and HR-C_1F_1, respectively

the dislocation accommodation and delays the strain concentration in the interface region, thus achieving better ductility.

Figure 7 shows the microstructures of the HCR-C_0F_1 revealed by TEM. It can be seen that the cryogenic rolling results in substantial dislocation multiplication and pile-ups (Figs. 7(a) and (c)). Moreover, some twins can be occasionally detected in the deformed Cu matrix (Fig. 7(a)), and some twin boundaries (TB) have been developed into sub-grain boundaries (SGB), which can be demonstrated by the inserted SAED image and HRTEM image in Fig. 7(a) as well as the SAED patterns (Fig. 7(b)) recorded from the region of twin boundary. Such observations indicate that the transformation from twin boundary to sub-grain boundary should be responsible for the grain refinement during the cryogenic rolling (Fig. 3). In addition, stacking faults (SFs) can be detected in the nearby region of the twin boundaries (insets in Fig. 7(a)) because stacking faults generally serve as nuclei for twins. Along with the evolution of the microstructure in the Cu matrix, the tight Cu−CNTs interface was retained in HCR-C_0F_1 (Fig. 7(c)).

Figure 8 displays the microstructures of HCR-C_1F_1 characterized by TEM. It can be seen that lots of

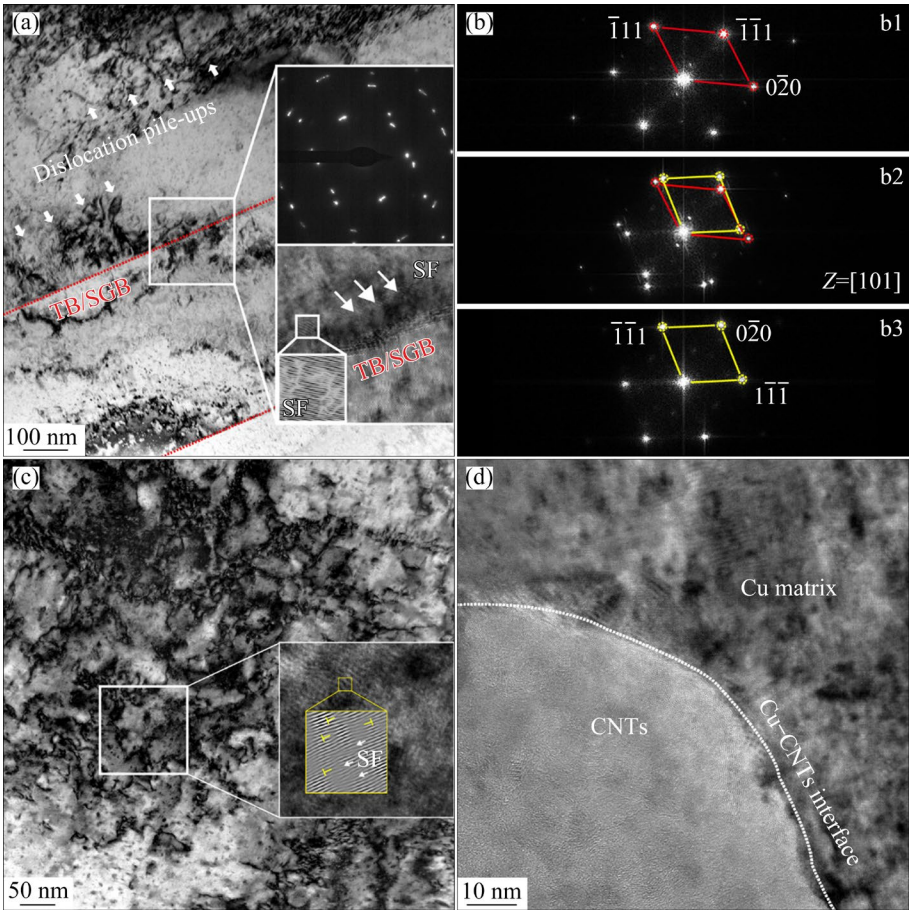

Fig. 7 Microstructures of HCR-C_0F_1 characterized by TEM: (a) BFTEM image of typical twin formed in HCR-C_0F_1 (The inserted SAED and HRTEM images are recorded from the twins); (b) SAED images recorded from upper grain (b1), twin boundary (b2), and lower grain (b3), respectively; (c) Representative BFTEM image of dislocation entangle in HCR-C_0F_1; (d) HRTEM image of Cu−CNTs interface

nanotwins and SFs were formed in the Cu matrix of HCR-C_1F_1 (Fig. 8(a)), as marked by the yellow and green arrows, respectively. The magnified BFTEM image (Fig. 8(b)) and HRTEM image (Fig. 8(c)) demonstrate that the twins have a width in the range from 3 to 30 nm. Moreover, the significant dislocation pile-ups were also induced near the multiple twins, approved by the inserted SAED pattern (Fig. 8(d)) and the corresponding HRTEM of the TB (Fig. 8(e)). The inverse fast Fourier transform (IFFT) image confirms that the multiplied dislocations entangle with each other and interact with the TB and SFs. In addition, similar to other composites, the tightly bonded interface between the Cu matrix and CNTs (Fig. 8(f)) is retained even though the HCR-C_1F_1 composite has experienced severe plastic deformation under low temperatures.

The above microstructure characterization results demonstrate that the inclusion of 50 wt.% coarse Cu powders can promote the formation of twins in the fabricated composites, especially when the cryogenic rolling is further applied after hot rolling, which can be explained by the following reasons. On the one hand, as widely demonstrated in the available literature [32,33], grain size is a key factor that affects the twin formation in metals and alloys during plastic deformation, and larger grain size facilitates the twin nucleation for conventional coarse-grained (CG) materials. So, the larger grain size of HR-C_1F_1 and HCR-C_1F_1 induced by the incorporation of 50 wt.% coarse Cu powders should be responsible for the twin formation in them. On the other hand, during the cryogenic rolling for preparing HCR-C_0F_1 and HCR-C_1F_1, the dislocation slide is significantly restricted due to the low temperature. As a result, twining as a deformation way is activated in the Cu matrix. Meanwhile, the uniformly dispersed CNTs should also promote the formation of nanotwins in the Cu matrix during the cryogenic rolling in the following aspects. Firstly,

the uniformly dispersed CNTs can induce lots of Cu−CNTs interface in the Cu matrix, which can promote partial emission from the Cu−CNTs interfaces, hence facilitating the formation of nanotwins [34]. Secondly, the incorporation of uniformly dispersed CNTs can substantially decrease the stacking fault energy of the Cu matrix, and the lowered stacking fault energy can make the nanotwins formation easier [19]. Therefore, the formation of nanotwins in HCR-C_1F_1 can be attributed to the combined effects of larger grain size, cryogenic rolling, and uniformly dispersed CNTs.

3.2 Mechanical properties

The uniaxial tensile tests were conducted to evaluate the mechanical properties of the HR-C_0F_1, HR-C_1F_1, HCR-C_0F_1, and HCR-C_1F_1. As presented in Fig. 9(a), the HR-C_1F_1 has lower yield strength (YS) but larger ductility than HR-C_0F_1, while the two

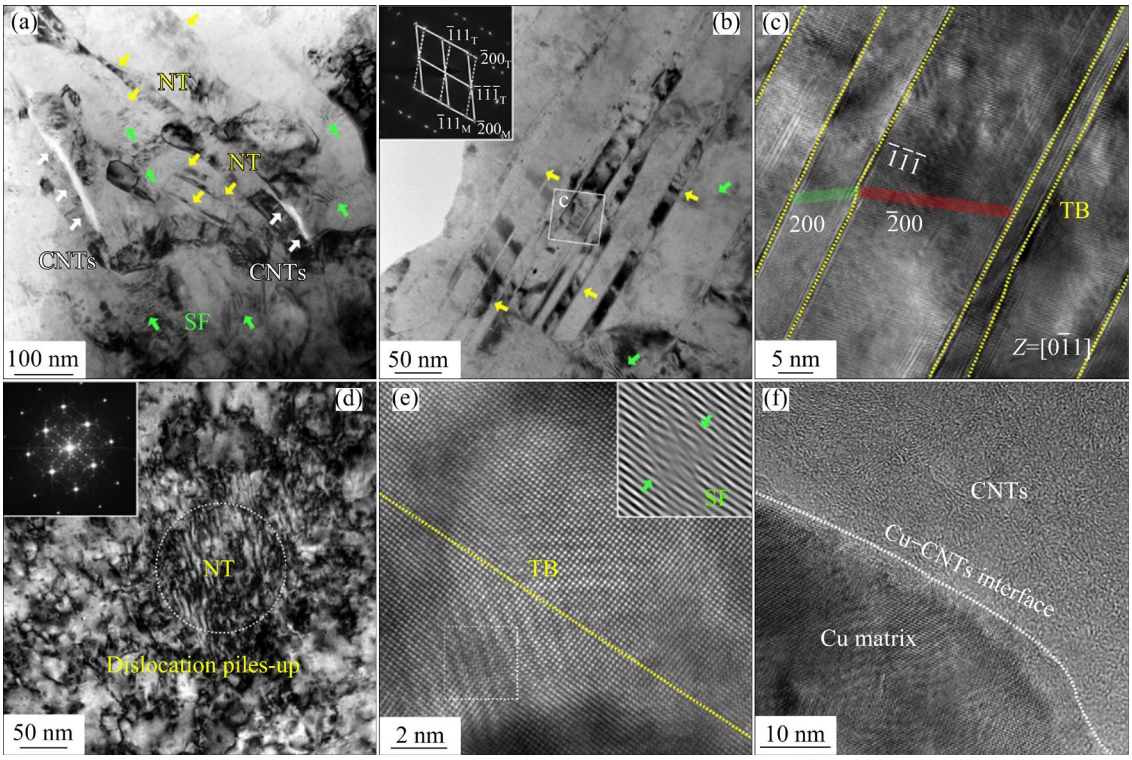

Fig. 8 Microstructures of HCR-C_1F_1 characterized by TEM: (a) BFTEM image with low magnification; (b) Enlarged BFTEM image of nano twins (NT) (The inset is SAED pattern of nanotwins); (c) HRTEM image of area marked by white square in (b); (d) Enlarged BFTEM image of coexisted nanotwins and multiplied dislocations (The insert is the SAED pattern of the multiple twins); (e) HRTEM image of nanotwins marked by white dashed circle in (d) (The inset is the IFFT image of Cu matrix near the TB); (f) HRTEM image of Cu−CNTs interface

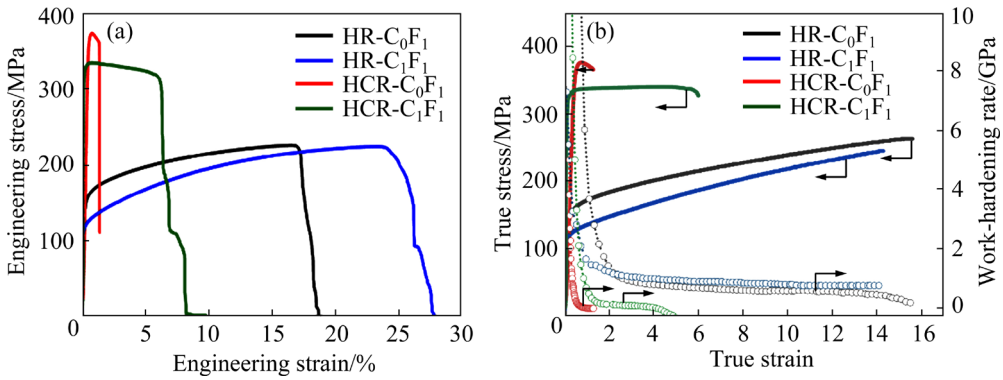

Fig. 9 Mechanical properties of fabricated composites: (a) Engineering stress−strain curves; (b) True stress−strain, and work-hardening rate curves

composites have comparable ultimate tensile strength (UTS). After cryogenic rolling, the YS of HCR-C_0F_1 is increased to (347.3±7.6) MPa, which is ~186.9 MPa higher than that of the HR-C_0F_1, but the elongation is substantially decreased to ~1.4%. Similarly, the YS of HCR-C_1F_1 is (336.6±8.5) MPa, which is ~229.1 MPa higher than that of the HR-C_1F_1. However, the tensile ductility of HCR-C_1F_1 is retained to be ~6.2%. The detailed values of the measured mechanical properties of these composites are illustrated in Table 2. The measured results of mechanical properties demonstrate that the incorporation of 50 wt.% coarse Cu powders when preparing the composite powders only slightly lowers the strength of the fabricated composites, but substantially improves their ductility, regardless of the hot-rolled or cryogenically-rolled state.

Figure 9(b) shows the true stress−strain curves and the strain-hardening rate curves of the four types of composites. It can be seen that the work-hardening rate of the cryogenically-rolled composites is much lower than that of the hot-rolled counterparts. Nevertheless, the HCR-C_1F_1 exhibits a homogeneous deformation stage before the appearance of strain-softening. Such plastic deformation characteristics should be the result of the offset between work-hardening induced by the interaction between dislocation and nanotwins, and the work-softening caused by the dislocation recovery [35].

Table 2 Mechanical properties of four specimens

Sample	YS/MPa	UTS/MPa	Elongation/%
HR-C_0F_1	160.4±9.2	225.5±10.9	17.1±0.6
HR-C_1F_1	107.5±10.5	226.3±8.6	23.9±0.7
HCR-C_0F_1	347.3±7.6	384.3±9.3	1.4±0.2
HCR-C_1F_1	336.6±8.5	345.1±7.6	6.2±1.3

Figure 10 presents the SEM images of the fractured surfaces of tensile failed HCR-C_0F_1 and HCR-C_1F_1. As can be seen, the HCR-C_0F_1 presents typical intergranular fracture features (Fig. 10(a)), while transgranular fractured Cu grains can also be observed on the fracture surface of HCR-C_1F_1 in addition to the intergranular fractured Cu grains (Fig. 10(b)). The additional transgranular fracture features should originate from the addition of 50 wt.% coarse Cu powders, which facilitates the achievement of better ductility. In addition, it can be seen that the pull-out CNTs from HCR-C_0F_1 (Fig. 10(c)) and HCR-C_1F_1 (Fig. 10(d)) are stretched straightly along the tensile direction and have sharp ends, implying that the CNTs play an effective load bearing role before the two composites fracture.

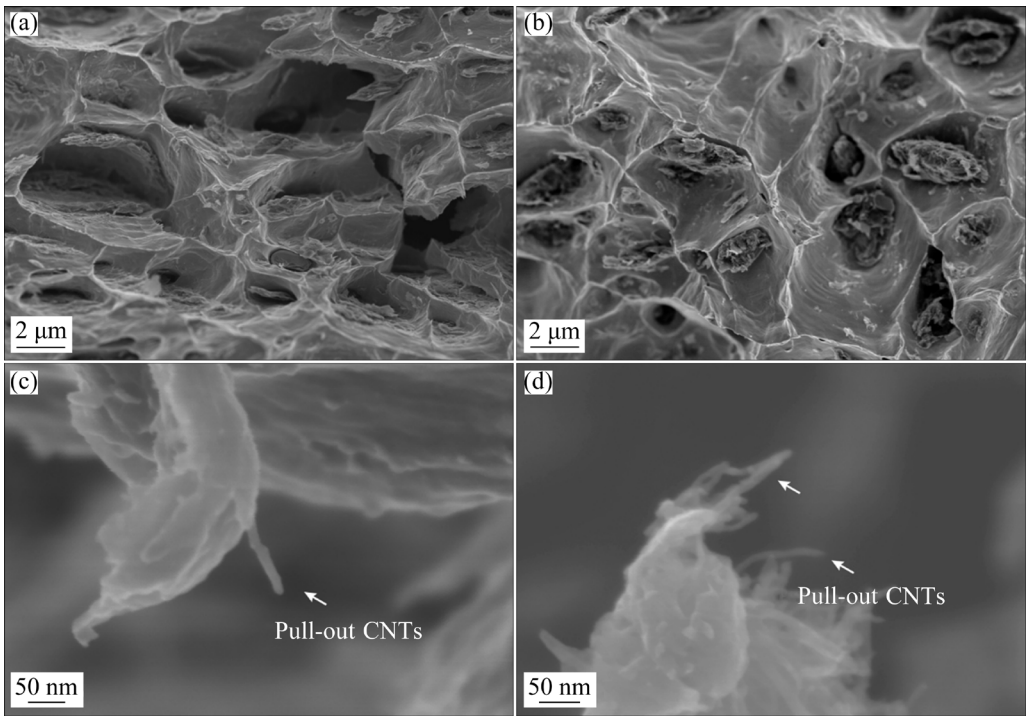

Fig. 10 SEM images of fractured surfaces of HCR-C_0F_1 (a, c) and HCR-C_1F_1 (b, d) after tensile failure tests

3.3 Strengthening and toughening mechanisms

To elucidate the fundamental reasons for the substantially improved strength and different ductility reductions of the HCR-C_0F_1 and HCR-C_1F_1 after cryogenic rolling, it is necessary to further analyze the involved strengthening and toughening mechanisms of these two composites. In general, the Orowan strengthening mechanism is important for the strength improvement of metal matrix composites. However, since the current hot-rolled and further cryogenically-rolled composites have similar CNTs dispersion, the Orowan strengthening mechanism should have a negligible contribution to the improved strength of the cryogenically-rolled composite over hot-rolled counterpart. According to the microstructure characterization results, the three main strengthening mechanisms should contribute to the improved strength, i.e., (1) grain refinement strengthening after cold rolling ($\Delta\sigma_{GR}$) [36], (2) dislocation strengthening due to the dislocation multiplication ($\Delta\sigma_{dis.}$) [19], and (3) nanotwins strengthening ($\Delta\sigma_{NT}$) [37]. Thus, assuming the YS of the cryogenically-rolled composites is the linear sum of the YS of the hot-rolled composites and the strength improvement originating from the strengthening mechanisms induced by cryogenic rolling, the YS of the HCR-C_0F_1 and HCR-C_1F_1 composites can be described as follows: $\sigma_{YS(HCR\text{-}C_0F_1)}=\sigma_{YS(HR\text{-}C_0F_1)}+\Delta\sigma_{GR}+\Delta\sigma_{dis.}+\Delta\sigma_{NT}$; $\sigma_{YS(HCR\text{-}C_1F_1)}=\sigma_{YS(HR\text{-}C_1F_1)}+\Delta\sigma_{GR}+\Delta\sigma_{dis.}+\Delta\sigma_{NT}$, where $\sigma_{YS(HR\text{-}C_0F_1)}$ and $\sigma_{YS(HR\text{-}C_1F_1)}$ denote the YS of the HR-C_0F_1 and HR-C_1F_1 composites, respectively.

The $\Delta\sigma_{GR}$ can be estimated based on the Hall−Petch relationship [38]:

$$\Delta\sigma_{GR}=K(D^{-0.5}-D_0^{-0.5}) \quad (1)$$

where K is the Hall−Petch slope (0.14 MPa·m$^{1/2}$ for FCC Cu [39]); D and D_0 are the average grain sizes of the composites before and after cryogenic rolling, respectively. Based on the grain information obtained from the EBSD results in Fig. 3(e), the $\Delta\sigma_{GR}$ of HCR-C_0F_1 and HCR-C_1F_1 composites are 61.6 and 40.2 MPa, respectively (Fig. 11).

The $\Delta\sigma_{dis.}$ can be estimated by the following equation according to the literature [40−42]:

$$\Delta\sigma_{dis.}=MaGb(\rho_{HCR}^{0.5}-\rho_{HR}^{0.5}) \quad (2)$$

where M is the Taylor factor of the pure Cu matrix (3.06 [2]); a is the lattice parameter of the pure copper matrix (0.361 nm [43]); G is the shear modulus of the Cu matrix and can be taken as 39 GPa [44]; b is the magnitude of Burgers vector of the Cu matrix and has a value of 0.255 nm [42]. ρ_{HCR} and ρ_{HR} are dislocation densities of the cryogenically-rolled composites and the hot-rolled composites, respectively. By substituting the dislocation density obtained from the EBSD analysis results into the above formula, the calculated $\Delta\sigma_{dis.}$ values for HCR-C_0F_1 and HCR-C_1F_1 composites are 117.9 and 143.4 MPa, respectively (Fig. 11).

Therefore, by calculating based on the equation: $\Delta\sigma_{NT}=\Delta\sigma_{YS(HCR)}-\Delta\sigma_{YS(HR)}-\Delta\sigma_{GR}-\Delta\sigma_{dis.}$, the strength contribution by nanotwins for HCR-C_0F_1 and HCR-C_1F_1 composites can be estimated to be 7.4 and 45.8 MPa, respectively (Fig. 11). Accordingly, the $\Delta\sigma_{NT}$ accounts for 3.9% and 19.9% of the overall increased strength for the HCR-C_0F_1 and HCR-C_1F_1 composites, respectively. Moreover, the proportion of the $\Delta\sigma_{GR}$ and $\Delta\sigma_{dis.}$ to the whole strength increment is 32.9% and 63.2% for HCR-C_0F_1 composite, while 17.5% and 62.6% for HCR-C_1F_1 composite, respectively (Fig. 11). Such theoretical calculation results demonstrate that the grain refinement strengthening and dislocation strengthening are the dominant strengthening mechanisms for HCR-C_0F_1, and the nanotwins strengthening is negligible. However, in addition to the grain refinement strengthening and dislocation strengthening, the nanotwins strengthening is also one of the main strengthening mechanisms for HCR-C_1F_1 composite.

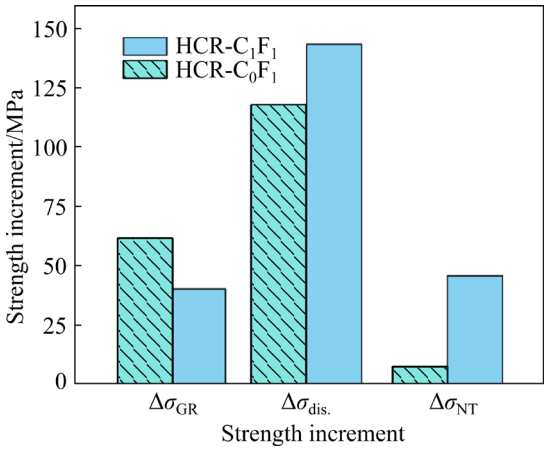

Fig. 11 Column figure summarizing strength increment contributions of involved strengthening mechanisms

In addition to the substantial strength increment after cryogenic rolling, it is surprising that HCR-C_1F_1 composite retains a much better tensile elongation than HCR-C_0F_1 composite, thus resulting

in higher synergy of strength and ductility of the CNTs reinforced Cu matrix composite, which can be attributed to the following reasons. Firstly, the HCR-C_1F_1 possesses a lower dislocation density than HCR-C_0F_1, which allows more dislocations to be accommodated during the tensile test. Secondly, the successful incorporation of nanotwins into HCR-C_1F_1 provides more space for accommodating the proliferated dislocation [45,46]. The higher dislocation accommodation space of HCR-C_1F_1 than HCR-C_0F_1 can delay the stress and strain concentration during the tensile test, thus helping achieve a much higher tensile strain.

4 Conclusions

(1) The incorporation of 50 wt.% coarse Cu powders when preparing the composite powders facilitates the formation of nanotwins in the fabricated CNTs reinforced Cu matrix composites, especially in the cryogenically-rolled composite.

(2) The hot-rolled composites (HR-C_0F_1 and HR-C_1F_1) without nanotwins have lower yield strength but higher tensile ductility, while the cryogenically-rolled composite without nanotwins (HCR-C_0F_1) has much higher tensile strength ((347.3±7.6) MPa) but extremely lower ductility ((1.4±0.2)%).

(3) The introduction of nanotwins in the CNTs reinforced Cu matrix composites not only helps to achieve substantially higher yield strength ((336.6±8.5) MPa) but also contributes to better tensile ductility ((6.2±1.3)%), resulting in better strength and ductility synergy.

(4) The strength increment originating from nanotwins is up to 19.9% of the overall strength increment for the composite after incorporating nanotwins. Good tensile ductility originates from the increased dislocation accommodation ability contributed by the formed nanotwins and lower induced dislocation proliferation.

CRediT authorship contribution statement

Wei-lin YU: Methodology, Data curation, Writing – Original draft; **Si-wei LUO:** Formal analysis, Investigation, Data curation; **Juan ZHU:** Data curation, Writing – Review and editing; **Min SONG:** Investigation, Supervision; **Tian-yu SUN:** Investigation, Formal analysis; **Jian-hong YI:** Supervision; **Liang LIU:** Investigation; **Yang-zhen LIU:** Investigation, Supervision; **Zhi-guo ZHANG:** Supervision; **Yong YANG:** Investigation, Supervision; **Zhen-tao YU:** Methodology, Supervision; **Wei LI:** Resources, Supervision; **Bai-song GUO:** Investigation, Funding acquisition, Formal analysis, Conceptualization，Writing – Review & editing, Supervision.

Declaration of competing interest

The authors declare that they have no known competing financial interests or personal relationships that could have appeared to influence the work reported in this paper.

Data availability

The raw/processed data can be provided by the corresponding author upon reasonable request.

Acknowledgments

This research was financially supported by the Fundamental Research Funds for the Central Universities, China (No. 21624408), the Guangdong Basic and Applied Basic Research Foundation, China (Nos. 2023A1515012850, 2024A1515010416), Guangzhou Science and Technology Planning Project, China (No. 2024A04J9966), the National Natural Science Foundation of China (Nos. 52271132, 52004101), and the Key Laboratory of Advanced Materials of Yunnan Province, China (No. 2024KF02).

References

[1] SRINIVASAN V, KUNJIAPPAN S, PALANISAMY P. A brief review of carbon nanotube reinforced metal matrix composites for aerospace and defense applications [J]. International Nano Letters, 2021, 11(4): 321−345.

[2] LUO Si-wei, CHEN Biao, SONG Min, ZHANG Zhi-guo, YI Jian-hong, ZHOU Sheng-feng, GUO Bai-song, YU Zhen-tao, LI Wei. Improving the strength-ductility synergy of carbon nanotubes reinforced Cu matrix composites through interfacial regulation [J]. Composites (Part A): Applied Science and Manufacturing, 2023, 175: 107787.

[3] LUO Si-wei, YU Wei-lin, SONG Min, YI Jian-hong, GUO Bai-song, YU Zhen-tao, LI Wei. Tailoring the interface with the in-situ formed chromium oxide and carbide for higher mechanical properties of copper matrix composites [J]. Ceramics International, 2023, 49(17): 28107−28117.

[4] LUO Si-wei, WU Yue, CHEN Biao, SONG Min, YI Jian-hong, GUO Bai-song, WANG Qi-wei, YANG Yong, LI Wei, YU Zhen-tao. Effects of Cu content on microstructures and compressive mechanical properties of CNTs/Al−Cu composites [J]. Transactions of Nonferrous Metals Society of China, 2022, 32(12): 3860−3872.

[5] LIU Yang, TAO Jing-mei, LIU Yi-chun, HU Yong, BAO Rui,

LI Feng-xian, FANG Dong, LI Cai-ju, YI Jian-hong. Regulating the mechanical properties and electrical conductivity of CNTs/Cu composites by tailoring nano-sized TiC on the surface of intact CNTs [J]. Carbon, 2021, 185: 428−441.

[6] CHEN Xiao-feng, TAO Jing-mei, LIU Yi-chun, BAO Rui, LI Feng-xian, LI Cai-ju, YI Jian-hong. Interface interaction and synergistic strengthening behavior in pure copper matrix composites reinforced with functionalized carbon nanotube-graphene hybrids [J]. Carbon, 2019, 146: 736−755.

[7] GUO Kun-yu, XU Chang, LIN Xiao-ping, YE Jie, ZHANG Chong, HUANG Duo. Microstructure and strengthening mechanism of Mg−5.88Zn−0.53Cu−0.16Zr alloy solidified under high pressure [J]. Transactions of Nonferrous Metals Society of China, 2020, 30(1): 99−109.

[8] BAHADOR A, UMEDA J, HAMZAH E, YUSOF F, LI X C, KONDOH K. Synergistic strengthening mechanisms of copper matrix composites with TiO_2 nanoparticles [J]. Materials Science and Engineering: A, 2020, 772: 138797.

[9] ZHANG Si-ruo, KANG Hui-jun, WANG Zhi-cheng, GUO En-yu, CHEN Zong-ning, WANG Tong-min. Microstructure and properties of dual-scale particulate reinforced copper matrix composites with superior comprehensive properties [J]. Journal of Alloys and Compounds, 2021, 860: 157888.

[10] RITCHIE R O. The conflicts between strength and toughness [J]. Nature Materials, 2011, 10(11): 817−822.

[11] LU Ke, LU Lei, SURESH S. Strengthening materials by engineering coherent internal boundaries at the nanoscale [J]. Science, 2009, 324(5925): 349−352.

[12] LU Lei, CHEN Xian-hua, HUANG Xiao-xu, LU Ke. Revealing the maximum strength in nanotwinned copper [J]. Science, 2009, 323(5914): 607−610.

[13] ZHAO Huai-zhi, YOU Ze-sheng, TAO Nai-rong, LU Lei. Anisotropic toughening of nanotwin bundles in the heterogeneous nanostructured Cu [J]. Acta Materialia, 2022, 228: 117748.

[14] ZHANG Z Y, SUN L X, TAO N R. Nanostructures and nanoprecipitates induce high strength and high electrical conductivity in a CuCrZr alloy [J]. Journal of Materials Science & Technology, 2020, 48: 18−22.

[15] ZHAO Huai-zhi, YOU Ze-sheng, TAO Nai-rong, LU Lei. Anisotropic strengthening of nanotwin bundles in heterogeneous nanostructured Cu: Effect of deformation compatibility [J]. Acta Materialia, 2021, 210: 116830.

[16] CHENG Zhao, ZHOU Hao-fei, LU Qiu-hong, GAO Hua-jian, LU Lei. Extra strengthening and work hardening in gradient nanotwinned metals [J]. Science, 2018, 362(6414): eaau1925.

[17] CAO Z H, XU L J, SUN W, SHI J, WEI M Z, PAN G J, YANG X B, ZHAO J W, MENG X K. Size dependence and associated formation mechanism of multiple-fold annealing twins in nanocrystalline Cu [J]. Acta Materialia, 2015, 95: 312−323.

[18] MA Shuo, FU Li-ming, SHAN Ai-dang. Enhancing strength−ductility of the aluminum bronze alloy by generating high-density ultrafine annealing twins [J]. Materials Characterization, 2021, 177: 111057.

[19] GUO Bai-song, SONG Min, ZHANG Xin-ming, LIU Yang-zhen, CEN Xi, CHEN Biao, LI Wei. Exploiting the synergic strengthening effects of stacking faults in carbon nanotubes reinforced aluminum matrix composites for enhanced mechanical properties [J]. Composites (Part B): Engineering, 2021, 211: 108646.

[20] GUO Bai-song, NI Song, YI Jian-hong, SHEN Ru-juan, TANG Zhong-hua, DU Yong, SONG Min. Microstructures and mechanical properties of carbon nanotubes reinforced pure aluminum composites synthesized by spark plasma sintering and hot rolling [J]. Materials Science and Engineering: A, 2017, 698: 282−288.

[21] WU Wen-qian, GUO Lin, GUO Bai-song, LIU Yong, SONG Min. Altered microstructural evolution and mechanical properties of $CoCrFeNiMo_{0.15}$ high-entropy alloy by cryogenic rolling [J]. Materials Science and Engineering: A, 2019, 759: 574−582.

[22] LUO Kai-guang, WU Yu-ze, XIONG Han-qing, ZHANG Yun, KONG C, YU Hai-liang. Enhanced mechanical properties of aluminum matrix composites reinforced with high-entropy alloy particles via asymmetric cryorolling [J]. Transactions of Nonferrous Metals Society of China, 2023, 33(7): 1988−2000.

[23] FAN Cai-he, LI Yi-hui, WU Qin, OU Ling, HU Ze-yi, NI Yu-meng, YANG Jian-jun. Effect of cold rolling deformation on microstructure evolution and mechanical properties of spray formed Al−Zn−Mg−Cu−Cr alloys [J]. Transactions of Nonferrous Metals Society of China, 2024, 34(8): 2442−2454.

[24] LUO Si-wei, CHEN Biao, SONG Min, YI Jian-hong, YU Zhen-tao, ZHANG Zhi-guo, LI Wei, GUO Bai-song. A novel Cr_2O_3 coated CNTs system: Synthesis, microstructure regulation, and characterization [J]. Materials Characterization, 2023, 203: 113069.

[25] LI Xian-long, GUO Bai-song, YU Xiang, YANG Chuang-chuang, ZHOU Sheng-feng, CUI Shao-gang, ZHANG Zhi-guo, LI Wei. Particle morphology dependence of the mechanical and electrical properties in the in-situ graphene reinforced Cu matrix composites [J]. Composites (Part A): Applied Science and Manufacturing, 2024, 179: 108032.

[26] ZHANG K, ALEXANDROV I V, VALIEV R Z, LU K. Structural characterization of nanocrystalline copper by means of X-ray diffraction [J]. Journal of Applied Physics, 1996, 80(10): 5617−5624.

[27] WANG Yun-peng, FU Rui-dong, JING Lei, LI Yi-jun, SANG De-li. Grain refinement and nanostructure formation in pure copper during cryogenic friction stir processing [J]. Materials Science and Engineering: A, 2017, 703: 470−476.

[28] CHEN Y J, ROVEN H J, GIREESH S S, SKARET P C, HJELEN J. Quantitative study of grain refinement in Al−Mg alloy processed by equal channel angular pressing at cryogenic temperature [J]. Materials Letters, 2011, 65(23/24): 3472−3475.

[29] CHOI S W, JEONG J S, WON J W, HONG J K, CHOI Y S. Grade-4 commercially pure titanium with ultrahigh strength achieved by twinning-induced grain refinement through cryogenic deformation [J]. Journal of Materials Science & Technology, 2021, 66: 193−201.

[30] LIU Ying-guang, ZHOU Jian-qiu, LING Xiang. Impact of grain size distribution on the multiscale mechanical behavior of nanocrystalline materials [J]. Materials Science and Engineering: A, 2010, 527(7/8): 1719−1729.

[31] HŸRCH M J, SNOECK E, KILAAS R. Quantitative

measurement of displacement and strain fields from HREM micrographs [J]. Ultramicroscopy, 1998, 74(3): 131−146.
[32] BARNETT M R. A rationale for the strong dependence of mechanical twinning on grain size [J]. Scripta Materialia, 2008, 59(7): 696−698.
[33] LI Y, ZHAO Y H, LIU W, XU C, HORITA Z, LIAO X Z, ZHU Y T, LANGDON T G, LAVERNIA E J. Influence of grain size on the density of deformation twins in Cu−30%Zn alloy [J]. Materials Science and Engineering: A, 2010, 527(16/17): 3942−3948.
[34] YANG Wen-shu, DONG Rong-hua, JIANG Long-tao, WU Gao-hui, HUSSAIN M. Unstable stacking faults in submicron/micron Al grammins in multi-SiC_p/multi-Al nanocomposite [J]. Vacuum, 2015, 122: 1−5.
[35] UNGÁR T, LI L, TICHY G, PANTLEON W, CHOO H, LIAW P K. Work softening in nanocrystalline materials induced by dislocation annihilation [J]. Scripta Materialia, 2011, 64(9): 876−879.
[36] CHOI H J, MIN B H, SHIN J H, BAE D H. Strengthening in nanostructured 2024 aluminum alloy and its composites containing carbon nanotubes [J]. Composites (Part A): Applied Science and Manufacturing, 2011, 42(10): 1438−1444.
[37] JIN Z H, GUMBSCH P, ALBE K, MA E, LU K, GLEITER H, HAHN H. Interactions between non-screw lattice dislocations and coherent twin boundaries in face-centered cubic metals [J]. Acta Materialia, 2008, 56(5): 1126−1135.
[38] ZHANG Xiao-dan, HANSEN N, GAO Yu-kui, HUANG Xiao-xu. Hall−Petch and dislocation strengthening in graded nanostructured steel [J]. Acta Materialia, 2012, 60(16): 5933−5943.
[39] LI Dan-yang, FAN Guo-hua, HUANG Xiao-xu, JUUL JENSEN D, MIAO K, XU Chao, GENG Lin, ZHANG Yu-bin, YU Tian-bo. Enhanced strength in pure Ti via design of alternating coarse- and fine-grain layers [J]. Acta Materialia, 2021, 206: 116627.
[40] YE You-xiong, YANG Xu-yue, LIU Chen-ze, SHEN Yang-zhi, ZHANG Xiang-kai, SAKAI T K. Enhancement of strength and ductility of Cu−Sn−Zn alloy by iron addition [J]. Materials Science and Engineering: A, 2014, 612: 246−252.
[41] TANG Yan-chuan, KANG Yong-lin, YUE Li-juan, JIAO Xiao-liang. Mechanical properties optimization of a Cu−Be−Co−Ni alloy by precipitation design [J]. Journal of Alloys and Compounds, 2017, 695: 613−625.
[42] BAN Yi-jie, GENG Yong-feng, HOU Jin-rui, ZHANG Yi, ZHOU Meng, JIA Yan-lin, TIAN Bao-hong, LIU Yong, LI Xu, VOLINSKY A A. Properties and precipitates of the high strength and electrical conductivity Cu−Ni−Co−Si−Cr alloy [J]. Journal of Materials Science & Technology, 2021, 93: 1−6.
[43] XU Si-yang, LI Ying-long, ZHANG Mu-xin, SONG Tao, DING Hua, JING Song-yang. Improving strength and elongation combination of Cu−9Ni−6Sn−(0.2Nb) alloys by pre-annealing and aging treatment [J]. Materials Science and Engineering: A, 2022, 860: 144221.
[44] GUO Bai-song, LUO Si-wei, WU Yue, SONG Min, CHEN Biao, YU Zhen-tao, LI Wei. Regulating the interfacial reaction between carbon nanotubes and aluminum via copper nano decoration [J]. Materials Science and Engineering: A, 2021, 820: 141576.
[45] ZHANG Y X, WANG J J, TAO N R. Tensile ductility and deformation mechanisms of a nanotwinned 316L austenitic stainless steel [J]. Journal of Materials Science & Technology, 2020, 36: 65−69.
[46] LI Kun-mao, LIU Xiao-chun, LIU Yu-jing, WU Xiang, ZHANG Wen-cai, YANG Jun-jie, LI Wei, ZHOU Sheng-feng. Strengthening layer with nano-twins in titanium alloy induced by laser surface re-melting: Mechanism of high strength and ductility [J]. Materials Characterization, 2023, 196: 112632.

通过引入纳米孪晶提高 Cu/CNTs 复合材料的力学性能

余炜琳[1]，罗思伟[1]，朱 娟[1]，宋 旼[2]，孙天宇[1]，易健宏[3]，刘 亮[3]，
刘洋赈[1]，张治国[1]，杨 勇[4]，于振涛[1]，李 卫[1]，郭柏松[1]

1. 暨南大学 先进耐磨蚀与功能材料研究院，广州 510632；
2. 中南大学 粉末冶金全国重点实验室，长沙 410083；
3. 昆明理工大学 材料科学与工程学院，昆明 650093；
4. 香港城市大学 工程学院 机械工程系，香港 999077

摘 要：为了发挥纳米孪晶和碳纳米管对铜基复合材料的综合强化作用，通过低温轧制和优化所用铜粉的初始粒径，将宽度为 3~30 nm 的纳米孪晶引入碳纳米管增强铜基复合材料中。仅用 0.2% (质量分数)碳纳米管增强的铜基复合材料中就形成了纳米孪晶，同时铜基体的位错密度显著增加，晶粒尺寸也显著细化，与无明显纳米孪晶形成的复合材料相比，其强度−延展性协同作用要好得多。强化和韧化机理分析表明，强度的提高来源于细晶强化、位错强化和纳米孪晶强化，其中，纳米孪晶引起的强度提高占复合材料整体强度提高的 19.9%；同时，良好的拉伸延展性是由于所形成的纳米孪晶位错容纳能力的提高及诱导位错扩散的降低。

关键词：铜基复合材料；碳纳米管；纳米孪晶；强度；延展性

(Edited by Wei-ping CHEN)